OPEN ACCESS



Disentangling the Hadronic Components in NGC 1068

Marco Ajello¹, Kohta Murase^{2,3,4}, and Alex McDaniel¹ Department of Physics and Astronomy, Clemson University, Clemson, SC 29631, USA

³ School of Natural Sciences, Institute for Advanced Study, Princeton, NJ 08540, USA

Abstract

The recent detection of high-energy neutrinos by IceCube in the direction of the nearby Seyfert/starburst galaxy NGC 1068 implies that radio-quiet active galactic nuclei can accelerate cosmic-ray ions. Dedicated multimessenger analyses suggest that the interaction of these high-energy ions with ambient gas or photons happens in a region of the galaxy that is highly opaque for GeV–TeV gamma rays. Otherwise, the GeV–TeV emission would violate existing constraints provided by the Fermi Large Area Telescope (LAT) and the Major Atmospheric Gamma Imaging Cherenkov. The conditions of high optical depth are realized near the central supermassive black hole (SMBH). At the same time, the GeV emission detected by the Fermi LAT is likely related to the galaxy's sustained star formation activity. In this work, we derive a 20 MeV–1 TeV spectrum of NGC 1068 using 14 yr of Fermi LAT observations. We find that the starburst hadronic component is responsible for NGC 1068's emission above ~500 MeV. However, below this energy, an additional component is required. In the 20–500 MeV range, the Fermi LAT data are consistent with hadronic emission initiated by non-thermal ions interacting with gas or photons in the vicinity of the central SMBH. This highlights the importance of the MeV band to discover hidden cosmic-ray accelerators.

Unified Astronomy Thesaurus concepts: Gamma-ray astronomy (628); AGN host galaxies (2017); Cosmological neutrinos (338)

1. Introduction

NGC 1068 is one of the brightest and most studied active galactic nuclei (AGNs). It also hosts intense star formation (a starburst). Located at a distance of ~10 Mpc (Courtois et al. 2013), it is classified as a Seyfert 2 galaxy because of the absence of broad emission lines in its optical spectrum (Shields & Oke 1975). However, broad lines have been detected in polarized light (Antonucci & Miller 1985). This observation represents one of the foundations of the AGN unification model (Urry & Padovani 1995) as it implies the presence of an obscuring medium (the torus) on parsec scales.

NGC 1068's prominent X-ray emission is well understood as due to photons from the accretion disk being upscattered to X-rays by a population of thermal electrons located above the accretion disk (the so-called corona; Galeev et al. 1979; Takahara 1979; Haardt & Maraschi 1991). This coronal emission is heavily reprocessed by the dense obscuring torus, which is observed nearly edge on (e.g., Bauer et al. 2015).

Recent observations (García-Burillo et al. 2016) with the Atacama Large Millimeter/submillimeter Array (ALMA) have resolved the torus, which is found to have a radius of 3.5 pc and a mass of $\sim 10^5 \, M_{\odot}$. Further ALMA observations have shown that a wide-angle AGN wind is currently interacting with a large fraction of the molecular torus (García-Burillo et al. 2019). CO observations indicate the presence of an AGN-driven massive ($> 10^7 \, M_{\odot}$) molecular outflow launched from the inner $\sim 100 \, \mathrm{pc}$ region, and a starburst ring located at

Original content from this work may be used under the terms of the Creative Commons Attribution 4.0 licence. Any further distribution of this work must maintain attribution to the author(s) and the title of the work, journal citation and DOI.

1.5 kpc, responsible for most of the galaxy's star formation rate of $\approx 20 \, M_{\odot} \, \mathrm{yr}^{-1}$ (Fluetsch et al. 2019).

The GeV gamma-ray emission of NGC 1068 has typically been ascribed to the star formation activity, which, through the creation of supernova remnants and pulsar wind nebulae, is able to accelerate cosmic rays (Ackermann et al. 2012; Ajello et al. 2020). Recently, neutrino emission from NGC 1068 has been reported by IceCube at a confidence level of 4.2σ in the 1–20 TeV energy range (IceCube Collaboration et al. 2022). In the same energy range, the Major Atmospheric Gamma Cherenkov (MAGIC; Lorenz & MAGIC Collaboration 2004) telescope reported only upper limits on TeV gamma-ray emission from NGC 1068. These upper limits demonstrate that the TeV gamma-ray flux of NGC 1068 is less than a tenth of the neutrino flux. This implies that the region of hadronic $(pp \text{ or } p\gamma)$ interactions producing the observed neutrinos should be highly opaque to GeV-TeV gamma rays because hadronic interactions inevitably produce neutrinos and gamma rays with similar energies. Multimessenger data suggest that the neutrino emission radius R is smaller than $\sim 30-100$ Schwartzschild radius ($R_{\rm S} \sim 0.2$ au for NGC 1068; Murase 2022). Such hidden sources have independently been predicted by the analyses of the all-sky neutrino flux and the diffuse isotropic gamma-ray background (Murase et al. 2016; Bechtol et al. 2017).

The conditions of high $\gamma\gamma \to e^+e^-$ optical depth $(\tau_{\gamma\gamma})$ are reached in the immediate vicinity of the central supermassive black hole (SMBH; e.g., Murase et al. 2016, 2020; Inoue et al. 2020). The GeV–TeV photons are then reprocessed to MeV energies through pair cascades and then leave the source with a spectrum that depends on the distance from the SMBH. For this reason, in this work, we extract a 20 MeV–1 TeV spectrum of

² Department of Physics; Department of Astronomy & Astrophysics; Center for Multimessenger Astrophysics, Institute for Gravitation and the Cosmos, The Pennsylvania State University, University Park, PA 16802, USA

⁴ Center for Gravitational Physics and Quantum Information, Yukawa Institute for Theoretical Physics, Kyoto University, Kyoto, Kyoto 606-8502, Japan Received 2023 July 5; revised 2023 August 16; accepted 2023 August 22; published 2023 September 12

NGC 1068 using 14.3 yr of Fermi Large Area Telescope (LAT; Atwood et al. 2009) observations and interpret it as the sum of two components: a low-energy cascade emission and a high-energy starburst emission. This paper is organized as follows: Section 2 describes the analysis of Fermi LAT data, Section 3 describes the modeling, while Section 4 summarizes the results. In this work, we adopt the standard cosmological parameters: $H_0 = 70 \, \mathrm{km \, s^{-1} \, Mpc^{-1}}$, $\Omega_M = 1 - \Omega_\Lambda = 0.3$.

2. Gamma-Ray Data Analysis

The gamma-ray data used in this analysis were collected over ~14.3 yr by the Fermi LAT between 2008 August 4 and 2022 December 1. The full analysis includes events with energies in the range 20 MeV-1 TeV. We define a $10^{\circ} \times 10^{\circ}$ region of interest (ROI) centered at the 4FGL coordinates of NGC 1068 (4FGL J0242.6-0000). We use the standard data filters (DATA QUAL > 0 and LAT CONFIG == 1) and select photons corresponding to the P8R3_SOURCE_V3 class (Atwood et al. 2013; Bruel et al. 2018). The analysis is performed using Fermipy (v1.2; Wood et al. 2017), which utilizes the underlying Fermitools (v2.2.0). The Galactic diffuse emission is modeled using the standard interstellar emission model (gll iem v07.fits) and the point-source emission is modeled using the 4FGL Data Release 3 (DR3) catalog (gll_psc_v28.fits; Abdollahi et al. 2020, 2022). In order to account for photon leakage from sources outside of the ROI due to the point-spread function (PSF) of the detector, the model includes all 4FGL sources within a $15^{\circ} \times 15^{\circ}$ region. The energy dispersion correction (edisp_bins = -1) is enabled for all sources except the isotropic component. The analysis is split between two energy regimes, the 20 MeV-50 MeV regime and the 50 MeV-1 TeV regime. At the 50 MeV-1 TeV regime we perform a joint likelihood analysis over the four PSF classes and use a maximum zenith angle of 90°. Each PSF type has a designated isotropic spectrum (iso_P8R3_SOURCE_V3_PS-Fi v1, for i ranging from 0 to 3) that is used in the analysis. For the 20-50 MeV regime, we adopt the more stringent zenith angle of 80° and do not differentiate among the different PSF classes. We model the extragalactic emission and residual instrumental background using iso_P8R3_SOURCE_V3_v1. txt. The diffuse emission models are available from the Fermi Science Support Center.⁵ During the analysis, NGC 1068 is modeled as a power-law source with free index and normalization. The spectral parameters of the Galactic diffuse component (index and normalization) and the normalization of the isotropic component are left free to vary, as are the normalizations of all 4FGL sources with test statistics (TS) ≥ 25 that are within 5° of the ROI center and all sources with TS \geq 500 and within 7°. The computation of the spectral energy distribution (SED) data points is performed using the sed() method provided in Fermipy. The spectrum in each energy bin is modeled assuming a power law with an index of 2 while allowing the normalization of the source to vary. Upper limits are reported at the 95% confidence level and are calculated using the Bayesian method (Helene 1983). The spectral data from the Fermi LAT analysis are listed in Table 1. In Figure 1 we show an image of NGC 1068 from the European Southern Observatory's Very Large Telescope (VLT)⁶ overlaid with the 95% positional uncertainty ellipse for the 50 MeV-1 TeV

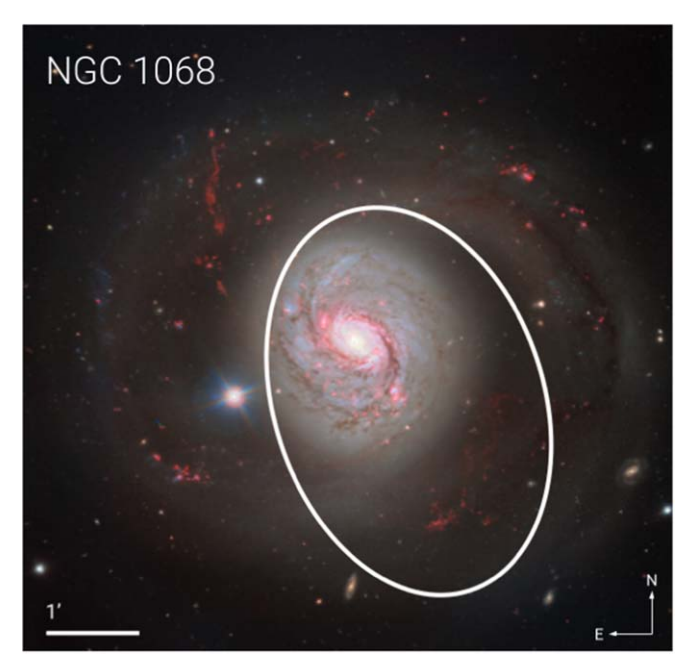


Figure 1. A 95% positional uncertainty ellipse for NGC 1068 in the 50 MeV–1 TeV energy range as derived in this analysis overlaid on an image from the VLT.

Table 1
SED Values for NGC 1068 between 20 MeV and 1 TeV

E (GeV)	Flux (erg cm ⁻² s ⁻¹)	TS
0.02-0.05	$< 3.20 \times 10^{-12}$	0.00
0.05-0.10	$2.13 \pm 0.60 \times 10^{-12}$	10.23
0.10-0.32	$1.56 \pm 0.26 \times 10^{-12}$	52.76
0.32-1.00	$1.49 \pm 0.15 \times 10^{-12}$	183.48
1.00-3.16	$8.70^{+1.06}_{-1.12} \times 10^{-13}$	159.82
3.16-10.00	$4.99^{+1.07}_{-1.21} \times 10^{-13}$	56.90
10.00-31.62	$5.86^{+1.67}_{-2.03} \times 10^{-13}$	51.11
31.62-100.00	$< 1.90 \times 10^{-13}$	0.00
100.00-1000.00	$4.95^{+3.36}_{-4.81} \times 10^{-13}$	7.86

Note. Upper limits are reported at the 95% confidence level and are computed using the Bayesian method.

analysis obtained using the localize() function in Fermipy. The measured spectrum of NGC 1068, shown in Figure 2, is in agreement with the one reported in the 4FGL-DR3 catalog (Abdollahi et al. 2022) and extends it to lower and higher energies, respectively.

3. Models and Implications

3.1. Starburst Galaxies

NGC 1068 is one of the starburst galaxies detected by the Fermi LAT (Ackermann et al. 2012; Ajello et al. 2020), and it was also considered to be among the most promising sources of PeV neutrinos (Lamastra et al. 2016; Murase & Waxman 2016). The starburst region is considered to be transparent to GeV—TeV gamma rays, and the observed GeV gamma-ray emission presumably comes from the decay of neutral pions, although the neutrino flux that modeling predicts would be associated with the gamma-ray emission is too low to explain the IceCube data.

⁵ https://fermi.gsfc.nasa.gov/ssc/

⁶ https://www.eso.org/public/images/eso1720a/

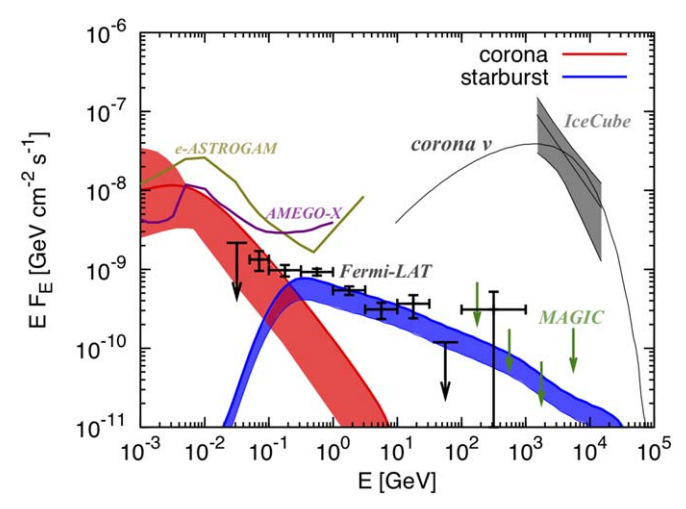


Figure 2. Model spectra of MeV–TeV gamma-ray emission from NGC 1068, compared to Fermi LAT data obtained by this work (black data points). AGN corona (Murase et al. 2020; Murase 2022) and starburst (Ajello et al. 2020; and see also the main text) models are shown by red and blue shaded bands, respectively. The all-flavor coronal neutrino spectrum, which can account for the IceCube data (gray shaded band; IceCube Collaboration et al. 2022), is also shown with the black thin solid curve (Murase et al. 2020). Sensitivity curves of AMEGO-X (Caputo et al. 2022) and e-ASTROGAM (De Angelis et al. 2017) are also overlaid.

Assuming that the starburst region is nearly calorimetric (see, e.g., McDaniel et al. 2023), we calculate the gamma-ray emission produced by cosmic rays via inelastic pp interactions with interstellar gas, adopting the method used in Murase (2022). The normalization of the starburst model is set by the $L_{\gamma}-L_{\rm IR}$ relation obtained by Ajello et al. (2020), where $\log_{10}L_{\rm IR}=10.97^7$ is used for NGC 1068 (Sanders et al. 2003). In Figure 2, we show the 2σ uncertainty bands for the starburst model. It is known that pionic gamma rays have a spectral break around 0.1 GeV below which the gamma-ray spectrum falls as $EF_E \propto E^2$. Figure 2 shows an excess of the data over the starburst model, particularly for energies at $\lesssim 500 \, {\rm MeV}$.

We also note that GeV gamma-ray emission could be produced by cosmic rays accelerated by AGNs, perhaps through disk winds (Liu et al. 2018; Ajello et al. 2021). Indeed, the source luminosity as predicted by the L_{γ} - $L_{\rm IR}$ relation slightly underestimates the true luminosity measured by Fermi LAT (see also Yoast-Hull et al. 2014). Inoue et al. (2022) proposed that the observed GeV gamma-ray emission may originate from interactions between the disk wind and the dusty torus. However, the sub-GeV excess exists even for these scenarios as long as the primary gamma-ray emission is produced primarily by hadronuclear interactions. Finally, in starburst galaxies, the leptonic component is subdominant to the hadronic one and its spectrum is harder than the excess observed here (Yoast-Hull et al. 2014; Peretti et al. 2019).

3.2. AGN Coronae

The excess of $\lesssim 500\,\text{MeV}$ gamma-ray emission shown in Figure 2 suggests the presence of another component at these energies. It may be a hint of gamma-ray emission from the coronal regions around the AGN accretion disk. It is widely believed that a hot, strongly magnetized plasma, the

so-called "corona," may produce X-ray emission through Compton upscattering of disk photons (Galeev et al. 1979; Haardt & Maraschi 1991). Recent global magnetohydrodynamic simulations (e.g., Jiang et al. 2019) and particle-incell simulations (e.g., Groselj et al. 2023) have demonstrated that such magnetically powered coronal regions naturally form as a result of magnetic dissipation in the black hole accretion system.

Murase et al. (2020) proposed the magnetically powered corona model for multi-TeV neutrino emission in which cosmic rays are accelerated by magnetic dissipation and the resulting turbulence in the vicinity of SMBHs. High-energy protons interact with optical/UV photons from the accretion disk and X-rays from the corona via $p\gamma$ interactions as well as the coronal gas via pp interactions. They showed the importance of Bethe-Heitler pair production for the energy losses of the protons making TeV neutrinos, as well as calculated the cascade emission resulting from synchrotron, inverse Compton, and two-photon annihilation. The model not only explains the multi-TeV neutrino flux of NGC 1068 but also the all-sky neutrino intensity in the 10 TeV range; furthermore, it predicts the associated proton-induced cascade gamma-ray emission in the MeV range. The cascade emission largely originates from synchrotron emission for strongly magnetized coronae.

In Figure 2, the cascade gamma-ray spectrum of the magnetically powered corona model is taken from Murase et al. (2020), where an emission radius of $R=30\,R_{\rm S}$ and an intrinsic X-ray luminosity of $L_{\rm X}=(1-3)\times 10^{43}\,{\rm erg\,s^{-1}}$ are used. The corresponding neutrino spectrum explains the observed IceCube data for NGC 1068 (see Figure 2). Interestingly, the cascade gamma-ray emission accompanied by neutrinos may explain the sub-GeV excess indicated by our Fermi LAT analysis.

The break or cutoff energy of the coronal gamma-ray emission, which is set by $\tau_{\gamma\gamma}\sim 1$, depends on R and $L_{\rm X}$. While predictions for hadronic gamma-ray emission at $\sim 1-10\,{\rm MeV}$ energies are rather robust, the flux in the $\sim 0.1\,{\rm GeV}$ range can be lower for smaller values of R (Murase 2022). For this reason, in Figure 2, the red uncertainty band of the model includes the case of $R=3R_s$ (corresponding to the innermost stable circular orbit radius of a nonrotating black hole) and $L_{\rm X}=7\times 10^{43}\,{\rm erg\,s^{-1}}$ (corresponding to the maximum luminosity within the 1σ uncertainty of NuSTAR observations) and considers both the minimal pp and $p\gamma$ models in Murase (2022).

4. Summary and Discussion

In this work, we have measured the gamma-ray spectrum of NGC 1068 using 14.3 yr of Fermi LAT observations. We have, for the first time, extended the measurement to 20 MeV to constrain potential hadronic components whose gamma-ray emission is absorbed and reprocessed in the MeV band (Murase et al. 2020; Inoue et al. 2022). We have found that above \gtrsim 500 MeV, the NGC 1068 spectrum can be well explained as the product of star formation activity. This emission is mostly hadronic in origin, particularly in starburst galaxies like NGC 1068, which act nearly as proton calorimeters (Lacki et al. 2011). Indeed, in these galaxies, the primary and secondary leptonic components are subdominant to the π^0 -decay

This is the luminosity at a distance of 10 Mpc.

 $[\]overline{^{8}}$ The cosmic-ray pressure $P_{\rm CR}$ is set to 15%–50% of the virial pressure, adopting a distance of 10 Mpc.

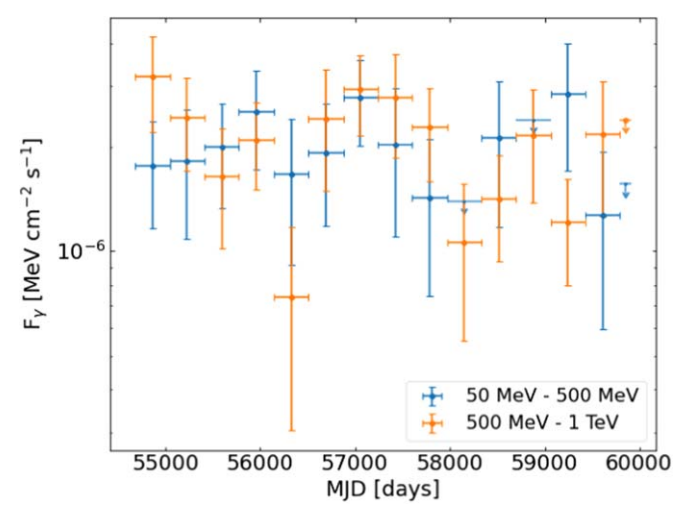


Figure 3. Yearly lightcurve of NGC 1068 at low (50-500 MeV, blue) and high (500 MeV-1 TeV, orange) energies.

component (Yoast-Hull et al. 2014; Peretti et al. 2019), although we do not exclude a potential contribution to the gamma-ray flux from electrons accelerated by outflows (Lenain et al. 2010; Lamastra et al. 2016). The low-energy (<500 MeV) part of the spectrum can be described by the proton-induced cascade emission from pp interaction and/or Bethe-Heitler pair-production processes in the AGN corona. This hadronic component is able to explain the low-energy Fermi and IceCube data at the same time, as shown in Figure 2. This implies that the two hadronic components that contribute to the NGC 1068 spectrum arise from different regions in the host

In the magnetically powered corona model (Murase et al. 2020), it is natural to expect time variability for coronal neutrino and gamma-ray emission. The minimum variability timescale can be the light-crossing time, R/c, which may range from minutes to hours. Longer variability timescales of days or longer—associated with dissipation, rotation, and accretion are also possible. To test this scenario, we extracted a lowenergy (50–500 MeV) and a high-energy (500 MeV-1 TeV) yearly (because of the low signal-to-noise ratio) binned lightcurve of the source. These lightcurves are reported in Figure 3 and show no evidence of variability (p-values of 0.40 and 0.15, respectively).

Furthermore, we note that the highest energy photon detected by the Fermi LAT within 0.25 deg of NGC 1068 (well within the 95% containment radius at >100 GeV) has an energy of 738 GeV. The second most energetic photon has an energy of 217 GeV. This shows that future observations by the Cherenkov Telescope Array (Actis et al. 2011) may detect the high-energy emission of NGC 1068.

MeV gamma-ray emission may also be produced by nonthermal electrons (Inoue et al. 2020). Particle acceleration mechanisms are currently uncertain, and not only stochastic acceleration in turbulence (Murase et al. 2020) but also magnetic reconnection (Kheirandish et al. 2021) and shock acceleration (Stecker et al. 1991; Inoue et al. 2020, 2022) have been proposed. Further multimessenger and multiwavelength studies, including MeV gamma-ray observations with, e.g., AMEGO-X (Caputo et al. 2022), will enable us to probe the

physics of dissipation and particle acceleration in the coronal regions.

Acknowledgments

M.A. and A.M. acknowledge support from NASA grant 80NSSC22K1580. Clemson University is acknowledged for the generous allotment of computer time on Palmetto cluster. K.M. is partly supported by the NSF grants No. AST-1908689, No. AST-2108466 and No. AST-2108467, and KAKENHI No. 20H01901 and No. 20H05852.

The Fermi LAT Collaboration acknowledges generous ongoing support from a number of agencies and institutes that have supported both the development and the operation of the LAT as well as scientific data analysis. These include the National Aeronautics and Space Administration and the Department of Energy in the United States, the Commissariat à l'Energie Atomique and the Centre National de la Recherche Scientifique/Institut National de Physique Nucléaire et de Physique des Particules in France, the Agenzia Spaziale Italiana and the Istituto Nazionale di Fisica Nucleare in Italy, the Ministry of Education, Culture, Sports, Science and Technology (MEXT), High Energy Accelerator Research Organization (KEK) and Japan Aerospace Exploration Agency (JAXA) in Japan, and the K. A. Wallenberg Foundation, the Swedish Research Council and the Swedish National Space Board in Sweden.

Additional support for science analysis during the operations phase is gratefully acknowledged from the Istituto Nazionale di Astrofisica in Italy and the Centre National d'Études Spatiales in France. This work was performed in part under DOE Contract DE-AC02-76SF00515.

ORCID iDs

Marco Ajello https://orcid.org/0000-0002-6584-1703 Kohta Murase https://orcid.org/0000-0002-5358-5642 Alex McDaniel https://orcid.org/0000-0002-8436-1254

References

Abdollahi, S., Acero, F., Ackermann, M., et al. 2020, ApJS, 247, 33 Abdollahi, S., Acero, F., Baldini, L., et al. 2022, ApJS, 260, 53 Ackermann, M., Ajello, M., Allafort, A., et al. 2012, ApJ, 755, 164 Actis, M., Agnetta, G., Aharonian, F., et al. 2011, ExA, 32, 193 Ajello, M., Baldini, L., Ballet, J., et al. 2021, ApJ, 921, 144 Ajello, M., Di Mauro, M., Paliya, V. S., et al. 2020, ApJ, 894, 88 Antonucci, R. R. J., & Miller, J. S. 1985, ApJ, 297, 621 Atwood, W. B., Abdo, A. A., Ackermann, M., et al. 2009, ApJ, 697, 1071 Atwood, W. B., Baldini, L., Bregeon, J., et al. 2013, ApJ, 774, 76 Bauer, F. E., Arévalo, P., Walton, D. J., et al. 2015, ApJ, 812, 116 Bechtol, K., Ahlers, M., Di Mauro, M., Ajello, M., & Vandenbroucke, J. 2017, ApJ, 836, 47 Bruel, P., Burnett, T. H., Digel, S. W., et al. 2018, arXiv:1810.11394 Caputo, R., Ajello, M., Kierans, C. A., et al. 2022, JATIS, 8, 044003 Courtois, H. M., Pomarède, D., Tully, R. B., et al. 2013, AJ, 146, 69 De Angelis, A., Tatischeff, V., Tavani, M., et al. 2017, ExA, 44, 25 Fluetsch, A., Maiolino, R., Carniani, S., et al. 2019, MNRAS, 483, 4586 Galeev, A. A., Rosner, R., & Vaiana, G. S. 1979, ApJ, 229, 318 García-Burillo, S., Combes, F., Ramos Almeida, C., et al. 2016, ApJL, 823, L12 García-Burillo, S., Combes, F., Ramos Almeida, C., et al. 2019, A&A, 632, A61 Groselj, D., Hakobyan, H., Beloborodov, A. M., Sironi, L., & Philippov, A. 2023, arXiv:2301.11327 Haardt, F., & Maraschi, L. 1991, ApJL, 380, L51

IceCube Collaboration, Abbasi, R., Ackermann, M., et al. 2022, Sci, 378, 538 Inoue, S., Cerruti, M., Murase, K., et al. 2022, arXiv:2207.02097

The significance of variability has been computed as in Appendix A.3 of Ajello et al. (2020).

```
Inoue, Y., Khangulyan, D., & Doi, A. 2020, ApJL, 891, L33
Jiang, Y.-F., Blaes, O., Stone, J. M., & Davis, S. W. 2019, ApJ, 885, 144
Kheirandish, A., Murase, K., & Kimura, S. S. 2021, ApJ, 922, 45
Lacki, B. C., Thompson, T. A., Quataert, E., et al. 2011, ApJ, 734, 107
Lamastra, A., Fiore, F., Guetta, D., et al. 2016, A&A, 596, A68
Lenain, J.-P., Ricci, C., Türler, M., Dorner, D., & Walter, R. 2010, A&A, 524, A72
Liu, R.-Y., Murase, K., Inoue, S., Ge, C., & Wang, X.-Y. 2018, ApJ, 858, 9
Lorenz, E. & MAGIC Collaboration 2004, NewAR, 48, 339
McDaniel, A., Ajello, M., & Karwin, C. 2023, ApJ, 943, 168
Murase, K. 2022, ApJL, 941, L17
Murase, K., Guetta, D., & Ahlers, M. 2016, PhRvL, 116, 071101
Murase, K., Kimura, S. S., & Mészáros, P. 2020, PhRvL, 125, 011101
```

```
Murase, K., & Waxman, E. 2016, PhRvD, 94, 103006
Peretti, E., Blasi, P., Aharonian, F., et al. 2019, MNRAS, 487, 168
Sanders, D. B., Mazzarella, J. M., Kim, D.-C., et al. 2003, AJ, 126, 1607
Shields, G. A., & Oke, J. B. 1975, ApJ, 197, 5
Stecker, F. W., Done, C., Salamon, M. H., & Sommers, P. 1991, PhRvL, 66, 2697
Takahara, F. 1979, PThPh, 62, 629
Urry, C. M., & Padovani, P. 1995, PASP, 107, 803
Wood, M., Caputo, R., Charles, E., et al. 2017, in Proc. 35th ICRC (ICRC2017), 301, 824
Yoast-Hull, T. M., Gallagher, J. S., Zweibel, E. G., & Everett, J. E. 2014, ApJ, 780, 137
```